Original Research Article

Development of Affordable Ceramic Microfiltration Membrane Using Rice Husk as a Pore Former for Brewery Water Treatment.

ABSTRACT

The creation of a flat microfiltration membrane using natural Nsu kaolinite clay and rice husk as a pore former was achieved using the solid state method of membrane preparation. The preparation conditions were the amount of kaolinite (5–15 wt%), sintering temperature (900–1100 ◦C) and sintering time (1-3 h) and response surface methods based on Box–Behnken design was employed in the membrane preparation. Optimization took place with the use of desirability function and the optimal membrane possesses the following characteristics: 44.4% porosity, 1566.6L $h^{-1}m^{-2}$ bar^{-1} of permeability, 35.97MPa mechanical strength and an average pore size of 0.8817 µm. The produced, optimized membrane was used in the purification, through microfiltration of brewery borehole water into brewery strike water and results show that Nsu kaolinite/ricehusk optimized membrane was able reduce turbidity, conductivity, total suspended solids and total dissolved solids to acceptable brewery standard with percentage of rejection of 83.8%, 77.7%, 90.5% and 73.00% respectively. The pH was also within the acceptable boundaries when it comes to brewery standard as most brewery strike water tend towards neutrality.

Keywords: Microfiltration, Nsukaolin, Rice husk, Strike water.

1 Introduction

The brewing industry is one of the most economically significant segments of the food industry, with an annual global beer production of around 1.34 billion hectoliters in 2002 [1]. With an average consumption of 23 litres/person per year, beer is the fifth most popular beverage in the world after carbonates, tea, milk, and coffee [2].Brewing maintains a crucial economic position in the food business in Nigeria. Due to the widespread consumption of beer, industry and research teams are working to create new technologies that will enable the production of high-quality, reasonably priced brews.

The world is facing a growing water crisis as freshwater resources are being depleted at an alarming rate. With only 2.5% of the Earth's water being freshwater, and less than 1% of it readily accessible, the scarcity of freshwater is becoming a pressing global concern [3]. According to Ajari et al [4], access to clean water is essential for human survival, but its scarcity has become a major issue due to pollution, urbanization, and waste mismanagement. Water is the most important chemical component of beer. According to Bamforth [5], the water utilized in a brewery is often considered a utility, but this water should be considered a raw material because it constitutes more than 90 % of the final beer. Majority of brewing process reactions occur in an aqueous solution, and thus beer products' qualities are directly impacted by the chemical properties of the water used. Such beer qualities often affected at every stage of manufacturing include: flavor, color, taste and turbidity [6;7]. Also the water properties affect brewing processes, such as fermentation and preservation [6;7].Potential and existing brewery water must meet the highest standards of purity and should also have a taste and odor that are acceptable to recommended quality standard [6]. Typically, brewery water

that passed quality standard has the following range of properties: turbidity (0-0.5 NTU), dissolved solid (20-50mg/l),suspended solids (30-61mg/l), pH(5-9.5), Colour (0.00 PCU), Conductivity (25-50µS/cm)[8].

Inorganic and polymeric membranes are the two different types of membranes for water filtration. In comparison to polymeric membranes, inorganic membranes offer additional benefits [9]. Polymeric membranes have a low chemical resistance, a specific solvent compatibility and are quickly exposed to dirt [10]. The major drawback of this membrane is its poor performance and thermal instability under severe operating conditions [11]. Nonetheless, because of their exceptional qualities, such as their great mechanical strength, high thermal stability, high chemical stability and long service life, inorganic membranes can be employed in severe situations [12].Ceramic membranes belong to the class of inorganic membranes. Typically, ceramic membranes are more expensive than polymer-based membranes. In order to produce commercial ceramic membranes, expensive raw materials like titania, zirconia, or alumina are typically used as inputs. In addition, their manufacturing costs are typically higher, with some commercial ceramic membranes costing over five times as much as polymeric membrane [13]. However, waste can be turned into a resource and used to save money on raw materials, protect the environment, and advance sustainable development if it is properly managed. In this regard, creating a stable low-cost ceramic membrane using readily available low-cost materials or industrial waste will significantly lower the cost of the membrane while preserving its exceptional characteristics and performance [10].

Membranes emerged as a viable means of water purification in the 1960s, since then, implementation of membranes for water treatment has progressed using more advanced membranes made from new and improved materials and applied in various configurations.

With applications in cold sterilization, tank bottom recovery, alcohol removal, as well as water and effluent treatment, membrane separation is gradually emerging as an alluring alternative processing method for the brewing sector [14]. Porous ceramic membrane (PCM) filtration has stood out among other technologies as a top contender for water treatment. PCMs can be made into various shapes using biomass and clays that are readily available in the area. For the preparation of PCMs, biomass sources like wheat, rice husks, wood flakes, and sawdust have been commonly used as burning additives. According to Hidouri et al [15], environmental analysis is becoming an increasingly important factor in system design. This biomas (ricehusk) is an agricultural waste and by recycling waste, we can conserve natural resources by reducing the need to procure and process new raw materials [16].These additives act as pore formers that burn off, thereby creating the required pores during firing in a furnace. [17-20].

In addition to reducing the amount of materials, energy, and time required, optimizing the experimental setup is also necessary to enhance membrane performance. One factor at a time optimization was used in the majority of experiments. This method takes a long time and necessitates a lot of trials. Response surface methodology (RSM) has garnered a lot of attention lately due to its ability to reduce the number of trials required and analyze all components at once, as well as the interactions that occur between the factors that are being studied. Specifically, RSM based on Box-Behnken design is mostly utilized because of its appealing benefits, which include the fact that it requires fewer experiments than three level complete factorial design and is more efficient than central composite design. When compared to this later, the Box-Behnken design makes it possible to avoid extreme experiment settings[21]

This current study intends to create a flat, porous ceramic micro-filtration (MF) membrane using rice husk (RH) [as a pore former] and Kaolin clay. This membrane will be applied in the purification of raw borehole water into brewery strike water. "Strike water" simply means the water that has been purified from natural sources to meet the standard required for brewing.

2 Materials and Methods

2.1 Raw materials sourcing and Instrumental characterization

Kaolin clay was obtained from Obo Nzu (Agbara-nzu) in Ehime-Mbano, Imo State while the rice husk was obtained from a rice farm at Amangwu, Edda in Afikpo South Local Government Area, Ebonyi State, Nigeria.

The TGA/DTA was performed on the kaolin using a TGA instrument (Make TGA 4000 Perkin Elmer) in order to investigate the thermal transition during sintering. Before starting the experiment, the "measure sample" icon was chosen, sample details such as the starting temperature, first temperature scan, first isothermal, second temperature scan was inputted in the Method Editor. The TGA was allowed to run. Maximum operating temperature was 1200℃ and max heat up rate put at 20℃. When the measurement was complete, the furnace was put in a cool position and the crucible containing the kaolin was removed.

The XRD patterns were carried out in an XRD equipment (Miniflex 600) for the kaolin sample Findings are frequently displayed as 2 peak positions and X-ray counts (intensity) in tables or x-y plots. The intensity (I) is either expressed as the intensity at the peak above the background or as the integrated intensity in the region beneath the peak. The ratio of the peak intensity to the intensity of the peak with the highest peak is used to calculate the relative intensity (relative intensity = I/I1 x 100). The XRF characterization was performed with

Genius IF instrument, kaolin and rice husk samples were all involved here. The WinTrace software's Acquisition Manager was used to construct a Method Tray List once the samples had been placed in the sample cups and placed on the sample tray. Along with a Method File, the Method Tray List would enable automated quantitative analysis. The first sample identification/analysis was entered into the Method Tray List, and the Method File was selected from the directory. The next sample was input on the following line after Acquisition Management opened the Method File and confirmed the sample position in the tray as being accurate. The Method File designated for the preceding sample is automatically filled out by the computer. This process went on until all of the samples had been used.

2.2 Preparation of rice husk cellulose

This procedure was also used by Singh [22] was adopted with minor alterations to suit this particular work.350g of rice husk was weighed into a 1000ml conical flask. 1500ml of 10%w/v sodium hydroxide (NaOH) was then poured into the flask and corked. The flask and its content were autoclaved at 121℃ at 15psi for 30minutes. It was then allowed to cool. After cooling, the fiber material was washed using distilled water. 500ml of 5% hydrogen peroxide was then added to the digested fiber and heated at 100℃ for 30minutes. The fiber was washed again using distilled water. After washing, 10% w/v sodium hypochlorite (NaClO) was added to the fiber (cellulose) to bleach it at 100℃ for 30minutes. The cellulose was washed finally using deionized water to remove color and ions until the effluent water was clear. The washed cellulose was dried in the oven at 80℃ for 3hours before increasing the temperature to 105℃ for 2hours for moisture removal. After drying, the cellulose was grinded and sieved to size of $\leq 50\mu m$ using standard sieve.

2.3 Membrane synthesis

The synthesis of porous ceramic membranes (PCMs) adopted here was the solid state method described by Segal [23] and Smart and Moore [24] with modifications. Mixtures of kaolin and cellulose were measured in the ratio of 95%, 90%, and 85% kaolin and 5%, 10% and 15% rice husk respectively. Deionized water was then added to the mixture of the kaolin and cellulose obtained according to Singh [22] at the ratio of 1:1 to obtain a homogenous consistency. The mixed samples were then cast in a prepared mold and oven dried at 105℃ for 24hours to form a disk membrane. The cast membranes were removed from the mold and transferred into the resistance muffle furnace. The membrane was calcined at 900℃, 1000℃ and 1100℃ for 1hour, 2hours and 3hours based on the experimental runs specified in box-behnken design. The resultant membrane was then cooled and soaked in water for 24hours to saturate the pores as well as avoid cracking before testing the membranes. Porosity of porous ceramic membrane was determined by a saturated water method[25] while water permeability of the produced membrane was obtained by a method used by Belgada et al [26].The calculation of compressive strength (N/cm^2) involved dividing the load (N) by the cross-sectional area (cm^2).

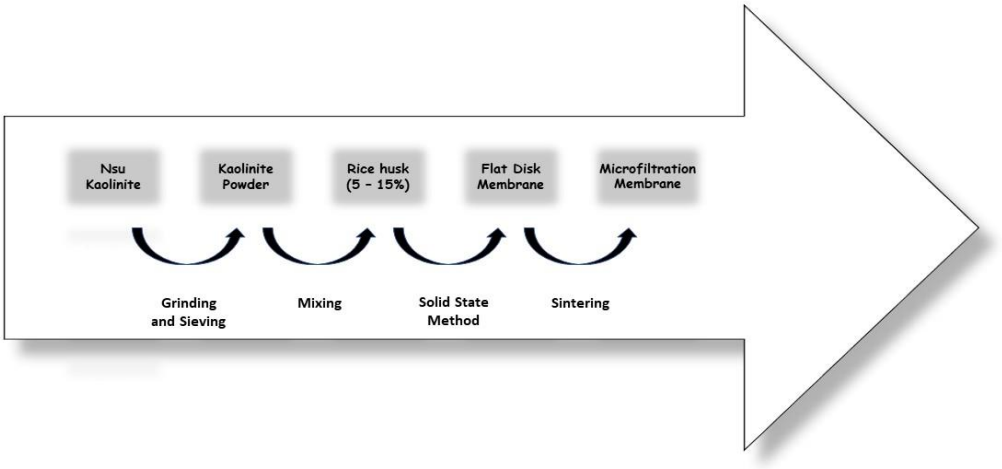

Fig.1: Schematic of the summary of the stages in membrane development

2.4 Experimental design and Procedure

RSM based on Box-Behnken design was employed in this study to evaluate the impact of preparation conditions on membrane performance and selected properties and to identify the impact of interaction effects. Sintering temperature (A), sintering duration (B) and mixture ratio (C), were chosen as factors while porosity (P), water permeability (WP) and mechanical strength (MS) of the membrane were taken into consideration as responses of the Box-Behnken design. The total number of experiments (N) were calculated using Eq. (1) below

$$N = 2k(k-1) + R_o \qquad (1)$$

Where k stands for the number of factors under investigation and R_O for the number of replicates in the center of the experimental domain. There are fifteen trials in total, three of which are duplicates of the center point. Table 1 shows clearly, the factors and their levels. The approach of least squares regression was utilized to model the experimental data. The

regression model's applicability was evaluated using ANOVA and the model fit test. Furthermore, three-dimensional visuals illustrating the interplay among the variables were obtained. To ascertain the ideal set of operational parameters for the membrane production, membrane optimization was also conducted.

Table 1: Independent factors and their levels

Factor	Name	Units	Type	SubType	Minimum	Maximum	Coded Low	Coded High	Mean	Std. Dev.
A	Temp	^{0}C	Numeric	Continuous	900.00	1100.00	-1 ↔ 900.00	+1 ↔ 1100.00	1000.00	75.59
B	Time	Hr	Numeric	Continuous	1.0000	3.00	-1 ↔ 1.00	+1 ↔ 3.00	2.00	0.7559
C	mixture ratio	%wt	Numeric	Continuous	5.00	15.00	-1 ↔ 5.00	+1 ↔ 15.00	10.00	3.78

2.5 Determination of membrane properties

2.5.1 Water permeability

Water permeability was conducted on a dead-end filtration setup with PCMs prepared at different conditions at constant pressure of 0.0017MPa. The permeability was determined by

the filtration of distilled water. The permeate flux J_w($Lh^{-1}m^{-2}$) and permeability Lp ($Lh^{-1}m^{-2}bar^{-1}$) Can be determined by equation 2 and equation 3 below.

$$\text{Permeate flux } (J_w) = \frac{V}{A.t} \quad (2)$$

while permeability is given as

$$\text{Permeability } (L_p) = \frac{J_w}{\Delta P} \quad (3)$$

Where V (L) is the volume of water passing through the membrane over the time t (h), A (m^2) is the surface area of the filtration and ΔP (bar) is the transmembrane pressure.

2.5.2 Pore volume and porosity

A saturated water method is used to determine the porosity of PCMs according to Halem[25]. To determine the water-saturated mass, a dry membrane sample is weighed, immersed in water for 24 hours, and then removed and weighed again. The pore volume and porosity of the membrane are given in equation (4) and (5) as

$$\text{Pore Volume} = \frac{\text{mass of wet membrane (Mw)} - \text{mass of dry membrane (Md)}}{\text{density of water}} \quad (4)$$

$$\text{Porosity} = \frac{\text{Pore volume of the membrane}}{\text{Total volume of the membrane}} \times 100 \quad (5)$$

2.5.3 Mechanical strength

Rectangular membrane samples with the same surface area and thickness as the flat disk membrane were created for mechanical strength tests. Then, flexural mechanical strength was determined using an ASTM C674-88-compliant 1 kN Shimadzu Screw Flat Grips based on a three-point bending load as expressed in equation (6) as

$$\text{Mechanical strength (MS)} = \frac{3PL}{2bd^2} \quad (6)$$

Where P (N) represents the maximum load at rupture, L (mm) represents the separation between the two supports, and b (mm) and d (mm), respectively, represent the width and thickness of the sample.

2.5.4 Microfiltration test

The optimized membrane performance was assessed by the filtration of raw borehole water at pressure of 0.08mPa.The raw borehole water was collected from Golden Guinea breweriesUmuahia, Abia state, Nigeria. Characterization of the raw water in terms of pH, turbidity, Colour,conductivity, Total dissolved solids and total suspended solid was carried out before and after the filtration experiment in order to determine the rejection Rx (%) of each parameter. Rejection is expressed as equation (7)

$$R_x = \left(1 - \frac{X_p}{X_f}\right) \times 100 \quad (7)$$

Where X_f and X_p are the characterization parameters before (feed) and after (product) filtration, respectively.

The physical structural change of the optimized samples were examined using scanning electron microscopy (SEM) utilizing the PhenomProX SEM model from phenomWorldEinhoven, the Netherlands. Sample was coated with 5nm of gold using a sputter coater by quorum technologies model Q150R after being placed on double adhesive that was on a sample stub. After viewing it through NaVCaM for focusing and minor adjustments, it was then transferred to SEM mode, where it was focused and the brightness and contrast were automatically adjusted. Then, the morphologies of various magnifications

were stored in a USB stick. ASTME 2809 (2022) was partly followed here. FTIR and XRD procedure was also carried out on the optimized membrane sample.

3.0 Results and Discussion

3.1 Thermal analysis of the Kaolin (Nsu Clay) (TGA/DTA)

Thermal analysis aims to pinpoint temperature ranges where kaolin weight losses (and hence transformations) are most prevalent. In order to evaluate the sample's thermal degradation behavior, it is necessary to analyze the impact of different temperature regimes on the kaolin material's porous structure, pore diameter, and mechanical strength. Figure 2 presents the TGA/DTA of the kaolinpowder. The dry inorganic sample was heated in an alumina crucible from ambient temperature to 1200 °C at a heating rate of 20 °C/min.Due to the presence of intricate phase transformations and interactions, the image illustrates the existence of a highly nonlinear variation. Between 25.5°C and 884.8°C, the kaolin material lost about 75.2 weight percent. From the TGA, there have essentially been two weight decreases. The first weight loss starts between 25.5°C and 270°C and is mostly caused by the loss of physisorbed water. The second starts between 320°C and 610°C which corresponds to dehydroxylation of kaolinite.

Kaolinite's thermal behavior is shown by DTA and Mohammadi and Pak [27] stated that the dehydroxylation reaction that transforms kaolin into amorphous metakaolin phase causes the peak at 380°C to be endothermic. This is evident in equation1 below. The peak between 600°C and 6350°C is exothermic, which is related to the crystallization of spinel [28]

$$Al_2O_3.2SiO_2.2H_2O(\text{kaolinite}) \rightarrow Al_2O_3.2SiO_2(\text{metakaonite}) + 2H_2O \quad (8)$$

The TGA curve indicated that the material did not experience any appreciable weight loss above 843 °C, consequently, the minimum sintering temperature for the production of the membrane should be higher than 843 °C.

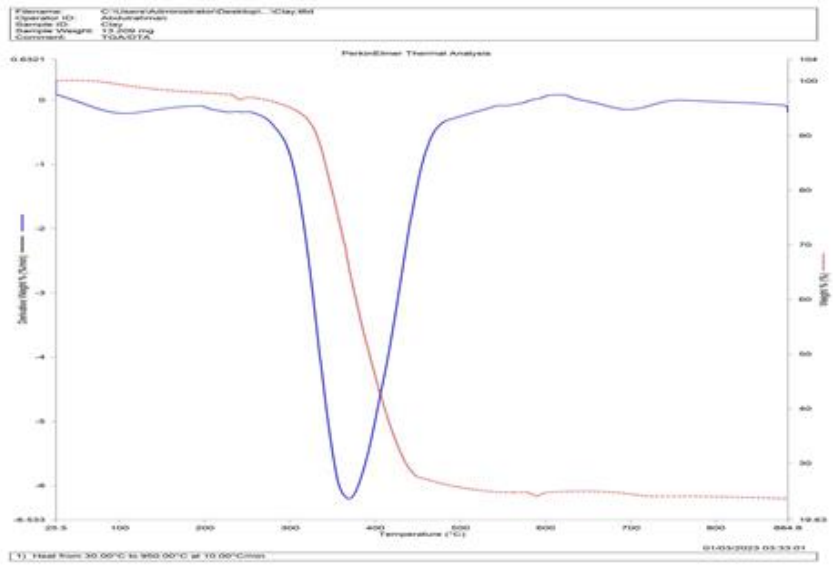

Fig. 2: TDA/DTA of Nsukaolin

3.2 Phase characterization by XRD analysis

The TGA-DTA analysis shows that essentially no substantial weight loss occurred above the sintering temperature of 884°C. An XRD investigation of clay structure at a temperature greater than 884 °C is performed to support this claim. Peaks and trends in the XRD chart in figure 3 shows that the inorganic mixture's primary constituents are mainly quartz, kaolinite, nacrite and illite with peaks of 467.52cts at 26.777^{o}2Th, 83.26cts at 12.51^{o}2Th,32.11cts at 39.59 ^{o}2Th and 69.90cts at 24.18^{o}2Th respectively, the structural changes that appeared on the Nsukaolin is awell-defined diffractions of kaolin clay at 2 theta values of 11.18-13.8°, 19.55-20.9°, and 24.8° commonly associated with kaolinite [29, 30]. However, the peaks

corresponding to the 2 Theta values of 21.5° and 27.6° are typical quartz properties [26]. Behnamfard *et al*. [32] established that kaoline mineralogical makeup contains quartz, which raises the silicon dioxide (SiO_2) level. In ceramic bodies and glazes, enormous amounts of quartz powder in form of $SiO_2$are employed. Quartz particles often behave as an embedded aggregate in bodies by remaining unmodified in the fired matrix. In porcelain bodies, they serve as the "skeleton", this property is a huge advantage in membrane production. No additional substantial phase shift occurs above 850 °C, according to a critical inspection of the peaks at higher temperatures. Nandi *et al*. [11] indicated that metakaolinite, a kind of quartz, makes up the majority of the membrane's skeletal structure. It is also clear from the XRD analysis that sintering temperatures above 850 °C are enough for membrane formation.

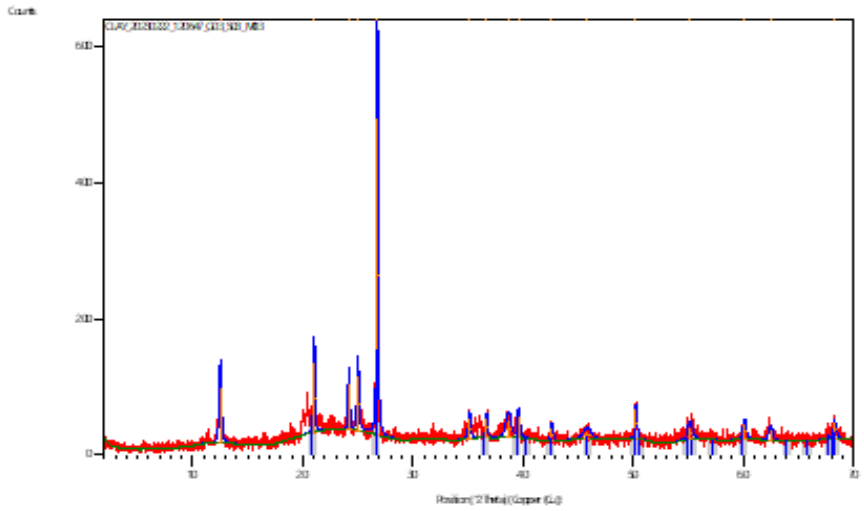

Fig. 3: X-ray diffraction (XRD) patterns of Nsukaolin

3.3 XRF Characterization of Nsu Clay (kaolin)

According to the results of an X-ray fluorescence (XRF) analysisshown in table 2 below, Nsu clay have high concentrations of SiO_2 (79.06 weight percent), significant concentrations of Al_2O_3 (10.05 weight percent), significant concentrations of SO_3 (3.48 weight percent) and Fe_2O_3 (2.90 weight percent), and lower concentrations of Cl (1.35 weight percent), CaO (1.34 weight percent), and TiO_2 (1.12 weight percent). K_2O, ZnO, and CuO are in negligible amounts.

Table 2: Chemical composition of Nsukaolin

Composition	Al_2O_3	SiO_2	SO_3	Fe_2O_3	Cl	CaO	TiO_2	K_2O	ZnO	CuO
Wt %	79.06	10.05	3.48	2.90	1.35	1.34	1.12	0.206	0.149	0.076

According to Garcia-Valles et al. [33], the Al_2O_3/Fe_2O_3 mass ratio may be utilized to identify, from an industrial perspective, the possible final uses of the clays in the formation of ceramic paste. Because of its greater Al_2O_3/Fe_2O_3 ratio and lower iron oxide content, Nsu kaolin is an excellent source of low-cost raw materials for making ceramic membranes for water filtering. The Aluminium and Iron oxides provide an excellent colloidal stability in clays [22].

3.4 XRF characterization of ricehusk

In the case of rice husk, presence of silca (SiO_2) plays a huge role in the fabrication of PCMs. Table 3 shows a higher percentage of silica in addition to similar constituents. The silica content of RH can play a role of the natural template for the formation of porous carbon

(PC).Tabata et al. [34] created an environmentally acceptable method for producing value-added hierarchical porous carbon (HPC) material that contains micro-, meso-, and macro-pores.Additionally, it has a wide range of significant uses in the industry for usage as adsorbents for membrane fabrication, suitable for water purification.

Table 3: Chemical constituents (in %) of the rice husk

Components					
CaO	SiO_2	Cl	Al_2O_3	Fe_2O_3	LOI
44.39	26.92	19.90	6.37	1.02	4.76

Determination of appropriate model

Table 4 shows the three factors of the Box-Behnken design and the corresponding responses from experiments. Examining the several models to identify the ones that best fit the experimental data allowed us to find the right model for predicting porosity, permeability, and mechanical strength.

Table 4: Three factors of the Box-Behnken design and the responses to them

	Factor 1	Factor 2	Factor 3	Response 1	Response 2	Response 3
Std Run	A:Temp	B:Time	C:mixture ratio	Porosity	Water Permeability	Mechanical Strength

		°C	Hr	%wt			
9	1	1000	1	5	36.6	1347	18.3
15	2	1000	2	10	33.3	1139	15
13	3	1000	2	10	35,3	1179	16
12	4	1000	3	15	33	933	31.8
2	5	1100	1	10	42.0	1421	12.2
6	6	1100	2	5	44.4	1409	24,7
4	7	1100	3	10	40.3	1524	30.9
5	8	900	2	5	41.6	2000	17.3
7	9	900	2	15	29.6	522	16.3
1	10	900	1	10	31.2	767	8.46
10	11	1000	3	5	41.7	1779	30.2
14	12	1000	2	10	34	1166	16.4
8	13	1100	2	15	39.8	1674	28
3	14	900	3	10	36.6	1364	10.2
11	15	1000	1	15	33.2	954	19,1

The importance of the values of the model equations for porosity, water permeability and mechanical strength were examined by F, R^2, adjusted R^2, lack-of-fit and adequate precision tests. For porosity, as shown in Table 6, the model F-value, which normally evaluated by dividing the mean squares of each variable response by the mean square, was 8.34, and a low probability value of 0.1116, which was less than p-value at the 95% confidence limit, signifies

that the model terms were significant. The model probability value of 0.0038 for water permeability and 010129 for mechanical strength also came out as low, enough to confirm that the model terms for water permeability and mechanical strength were significant. The goodness-of-fits of the models were also tested by using the correlation coefficient R^2, which represented the real relationship among the selected factors and the percentage of the variability of the parameters [35].

Table 5 showed that the R^2 value of 0.9823 for porosity indicated that only 0.017% of the variation in the porosity response could not be explained by the model and the model fitted well with the observed data. The R^2 values of 0.9909 and 0.9936 for water permeability and mechanical strength respectively were also reasonably close to unity, therefore acceptable. The adjusted R^2 values for porosity, water permeability and mechanical strength were obtained as 0.9506, 0.9746 and 0.9792 respectively were all statistically reasonable. Lack-of-fit tests in Table 6 were also used to evaluate the model adequacy; an insignificant lack-of-fit is required here. The lack-of-fit values for porosity, water permeability and mechanical strength were 0.3442, 0.0638 and 0.2058 respectively, these values were statistically insignificant and showed that the constructed models were consistent with the observations. The values of adequate precision displayed in Table 7 indicated that the signal-to-noise ratio, were 17.12, 29.22 and 24.00 for porosity, water permeability and mechanical strength respectively, the values being greater than 4 indicated a robust, significant and reliable signal. Fig. 4 shows that the points of the predicted vs. actual plots for porosity, water permeability and mechanical strength observations were aligned along a diagonal line, showing a strong correlation between predicted and observed values.

Table 5: Summary of model fit results for membrane properties

Porosity						
Source	**Std. Dev.**	**R^2**	**Adjusted R^2**	**Predicted R^2**	**PRESS**	
Linear	2.69	0.7226	0.6470	0.4857	147.13	
2FI	2.40	0.8391	0.7184	0.4783	149.25	
Quadratic	**1.01**	**0.9823**	**0.9506**	**0.8164**	**52.51**	**Suggested**
Cubic	1.01	0.9928	0.9496		*	Aliased
Permeability						
Source	**Std. Dev.**	**R^2**	**Adjusted R^2**	**Predicted R^2**	**PRESS**	
Linear	300.84	0.5343	0.4073	0.0222	2.090E+06	
2FI	124.36	0.9421	0.8987	0.7739	4.833E+05	
Quadratic	**62.22**	**0.9909**	**0.9746**	**0.8605**	**2.983E+05**	**Suggested**
Cubic	20.40	0.9996	0.9973		*	Aliased
MS						
Source	**Std. Dev.**	**R^2**	**Adjusted R^2**	**Predicted R^2**	**PRESS**	
Linear	**5.67**	**0.5916**	**0.4691**	**0.1218**	**691.87**	**Suggested**
2FI	5.87	0.6936	0.4309	-0.7712	1395.46	
Quadratic	**1.12**	**0.9936**	**0.9792**		*****	**Suggested**
Cubic	0.7211	0.9987	0.9914		*	Aliased

Table 6: Summary of Lack of fit test results for membrane properties

Porosity						
Source	**Sum of Squares**	**Df**	**Mean Square**	**F-value**	**p-value**	
Linear	77.30	9	8.59	8.34	0.1116	
2FI	43.98	6	7.33	7.12	0.1283	
Quadratic	**2.99**	**3**	**0.9975**	**0.9684**	**0.3442**	**Suggested**
Cubic	0.0000	0				Aliased
Permeability						
Source	**Sum of Squares**	**Df**	**Mean Square**	**F-value**	**p-value**	
Linear	9.947E+05	9	1.105E+05	265.47	0.0038	
2FI	1.229E+05	6	20481.89	49.20	0.0201	
Quadratic	**18525.75**	**3**	**6175.25**	**14.83**	**0.0638**	**Suggested**
Cubic	0.0000	0				Aliased
MS						
Source	**Sum of Squares**	**Df**	**Mean Square**	**F-value**	**p-value**	
Linear	**320.72**	**8**	**40.09**	**77.10**	**0.0129**	**Suggested**
2FI	240.40	5	48.08	92.46	0.0107	
Quadratic	**4.01**	**2**	**2.01**	**3.86**	**0.2058**	**Suggested**
Cubic	0.0000	0				Aliased

Table 7: Adequate Precision

Porosity	Water permeability	Mechanical Strength
17.12	29.22	24.00

(a) (b) (c)

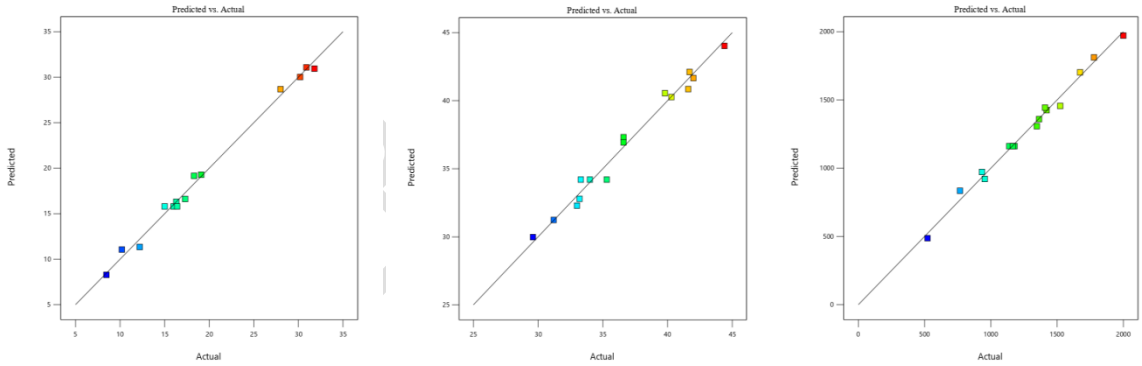

Fig.4: Graphical representation for the models (a) Porosity (b) water permeability (c) mechanical strength.

The proposed models for membrane properties were fitted into the actual experimental data obtained from the three-factor Box-Behnken design of the experiment to determine the relationship between the membrane independent variables and the expected responses. Multiple regression was used for model fitting and parameter estimation to derive the model

equation for respective responses in terms of the actual experiment. Equations (9), (10) and (11) represent porosity, water permeability and mechanical strength respectively.

$$\text{Porosity} = +311.25 - 0.572A + 20.275B - 5.1875C - 0.01775AB + 0.0037AC - 0.265BC + 0.000302A^2 + 0.3\square^2 + 0.065C^2 \quad (9)$$

$$Wp = +18720.8 - 30.1A + 1681B - 977.2C - 1.2AB + 0.87AC - 22.7BC + 0.013A^2 - 20.187\square^2 + 4.48C^2 \quad (10)$$

$$MS = -89.51 + 0.312A - 43B - 8.19C + 0.042AB + 0.0022AC + 0.04BC - 0.00018\square^2 + 1.146\square^2 + 0.30C^2 \quad (11)$$

These equations were used to predict the porosity, water permeability and mechanical strength of the membrane properties.

Table 8: Regression terms for porosity

Factor	Coefficient Estimate	Degree of Freedom	Sum of squares	F-value	P-value
Intercept	+311.25000		281.04	30.90	0.0007
A-Temperature	-0.572125	1	94.53	93.55	0.0002
B-Time	+20.27500	1	9.25	9.15	0.0293
C-Mixture ratio	-5.18750	1	102.96	101.89	0.0002
AB	-0.017750	1	12.60	12.47	0.0167

AC	+0.003700	1	13.69	13.55	0.0143
BC	-0.265000	1	7.02	6.95	0.0462
A^2	+0.000302	1	33.79	33.44	0.0022
B^2	+0.300000	1	0.3323	0.3289	0.5912
C^2	+0.065000	1	9.75	9.65	0.0267

Table 9: Regression terms for water permeability

Factor	Coefficient Estimate	Degree of Freedom	Sum of squares	F-value	P-value
Intercept	+18720.83333		2.118E+06	60.79	0.0001
A-Temperature	-30.09292	1	2.363E+05	61.04	0.0006
B-Time	+1681.04167	1	1.543E+05	39.85	0.0015
C-Mixture ratio	-977.16667	1	7.515E+05	194.11	< 0.0001
AB	-1.23500	1	61009.00	15.76	0.0106
AC	+0.871500	1	7.595E+05	196.17	< 0.0001
BC	-22.65000	1	51302.25	13.25	0.0149
A^2	+0.012783	1	60337.33	15.58	0.0109
B^2	-20.16667	1	1501.64	0.3879	0.5607
C^2	+4.48333	1	46385.26	11.98	0.0180

Table 10: Regression terms for mechanical strength

Factor	Coefficient Estimate	Degree of Freedom	Sum of squares	F-value	P-value
Intercept	-89.51000		782.81	68.86	0.0005
A-Temperature	+0.311625	1	177.56	140.57	0.0003
B-Time	-43.00000	1	253.58	200.74	0.0001
C-Mixture ratio	-8.18650	1	0.3605	0.2854	0.6215
AB	+0.042400	1	71.91	56.93	0.0017
AC	+0.002150	1	0.3528	0.2793	0.6251
BC	+0.040000	1	0.1600	0.1267	0.7399
A^2	-0.000182	1	6.66	5.27	0.0833
B^2	+1.45750	1	3.83	3.03	0.1566
C^2	+0.303700	1	188.18	148.97	0.0003

3.5 Analysis of variance

Table 11 displays the ANOVA findings for the models corresponding to porosity, water permeability, and mechanical strength for produced membrane. The model terms are

considered significant and suitable for prediction when the p-value is less than 0.05. This suggests that variations in the real physical factor values corresponding to a particular model term may have a substantial impact on the response under examination. According to Asfaram et al. [36], model terms that have p-values greater than 0.1 are considered non-significant, indicating that changes in the values of the physical element that the model term reflects do not significantly impact the response under investigation.

Table 11: Analysis of variance for porosity, permeability and mechanical strength

Response	Variation source	Df	Sum of squares	Mean square	F-ratio	P-values
Porosity	Regression	9	281.04	31.23	30.90	0.0007
	Residual	5	5.05	1.01		
	Total	14	286.9	32.24		
WP	Regression	9	2118000	235400	60.79	0.0001
	Residual	5	19358.42	3871.68		
	Total	14	2137358	239271.68		
MS	Regression	9	782.81	86.98	68.86	0.0005
	Residual	4	5.05	1.26		
	Total	13	787.86	88.24		

3.6 3D surface plots for interaction.

According to Adinaraya and Ellaiah [37], three-dimensional response surface plots, which display the relationship between two variables while holding the third constant are particularly useful for understanding the individual and interactive effects of the two variables

being studied. Furthermore, 3D response surfaces and their corresponding contour plots enable a clear and intuitive visualization of how experimental variables influence the responses, making it easier to analyze and interpret their effects [38]. To gain a deeper insight into how the independent variables and their interactions influence the dependent variable, the study generated 3D response surface based on the model equations (8-10), enabling a visual representation of these relationships. The curvatures was as result of the order of the polynomial which is quadratic in nature with gradient colors representing a continuous change in the response variable, with colours transiting from one shade or colour to another, the hotspots represent areas of maximum or minimum response, often indicated by bright colours or sharp colour changes, blue, yellow and red from minimum to maximum respectively in this study.

To better understand how the dependent and independent variables relate, contour plots were created. Since the regression model has three independent variables, one variable was fixed at its center level for each plot. This resulted in a 3D response plots and three corresponding contour plots for porosity, water permeability, and mechanical strength, as shown in Figure 4.According to Figure 5, variation of sintering temperature from 900℃ to 1100℃ leads to the increase of porosity (a) and permeability (b). However, this increase is more significant at high level of the amount of rice husk (15 wt%) (from 28.3% to 40.5% for porosity and from 499 to 1750 $Lh^{-1}m^{-2}bar^{-1}$ for permeability compared to the increase at low level (5 wt %) where the porosity slightly increases from 41.2% to 43.1% and permeability decreases from 1750 to 1400 $Lh^{-1}m^{-2}bar^{-1}$.The reverse is the case for mechanical strength which slightly increased at low level (5 wt %)(c).This significant increase for porosity and water permeability suggests that rice husk is a pore former. They burn during the sintered membrane process, creating pores. For permeability, they open pores and raises membrane flow, so an

increase in pore former directly affects permeability. Similar observation was made by Samhari, et al. [39]. Since rice husk created greater room after burning, it is evident that higher rice husk content improves the porosity of PCMs. Higher porosity was anticipated to increase the water filtration flow rate, but regrettably, it resulted in a major decrease in the mechanical strength at 28.2MPa.The creation of closure between pores, which results in the densification phenomena that is expected at this temperature range, could account for the decreased water permeability [40].

Conversely, when the mixture ratio is at a low level, the variation in sintering time from 1 to 3 hours, it significantly improves the permeability(e) and slightly improves the porosity(e) , moderate increase from 33.5% to 42% for porosity and water permeability increase from 1000 to 17500 $Lh^{-1}m^{-2}bar^{-1}$ was observed .This demonstrates that further sintering leads to a good phase rearrangement and robust grain connection as observed by Beqqour et al., [40]. But for mechanical strength, the higher value of 30 MPa was recorded (f). According to Dung et al [41], the amount of rice husk employed as a pore-forming agent can have a considerable impact on a ceramic membrane's porosity; a higher porosity could result in a decreased strength. Therefore, in order to maximize the performance of a ceramic membrane, its porosity and strength should be compromised.

There is a significant rise in mechanical strength from 10.2 to 32.7 MPa as a result of the variation in sintering temperature from 900 to 1100℃ at high sintering time of 3hours (g). Additionally, there is a moderate increase in permeability and a poor increase in porosity at these conditions. This anticipated behavior is mostly caused by the high degree of densification that occurs over time under the influence of sintering along with a significant

strengthening of the connections between grains [42]. On the other hand, when the sintering temperature is varied at a low level (1hour), it results in a slight increase in mechanical strength from 5.2 to 11.6 MPa and a significant increase in porosity from 26.7% to 41.9% (i), a strong increase in permeability from 350 to 1320 $Lh^{-1}m^{-2}bar^{-1}$(h) Partial densification brought on by the brief sintering period within the same temperature range may account for this.

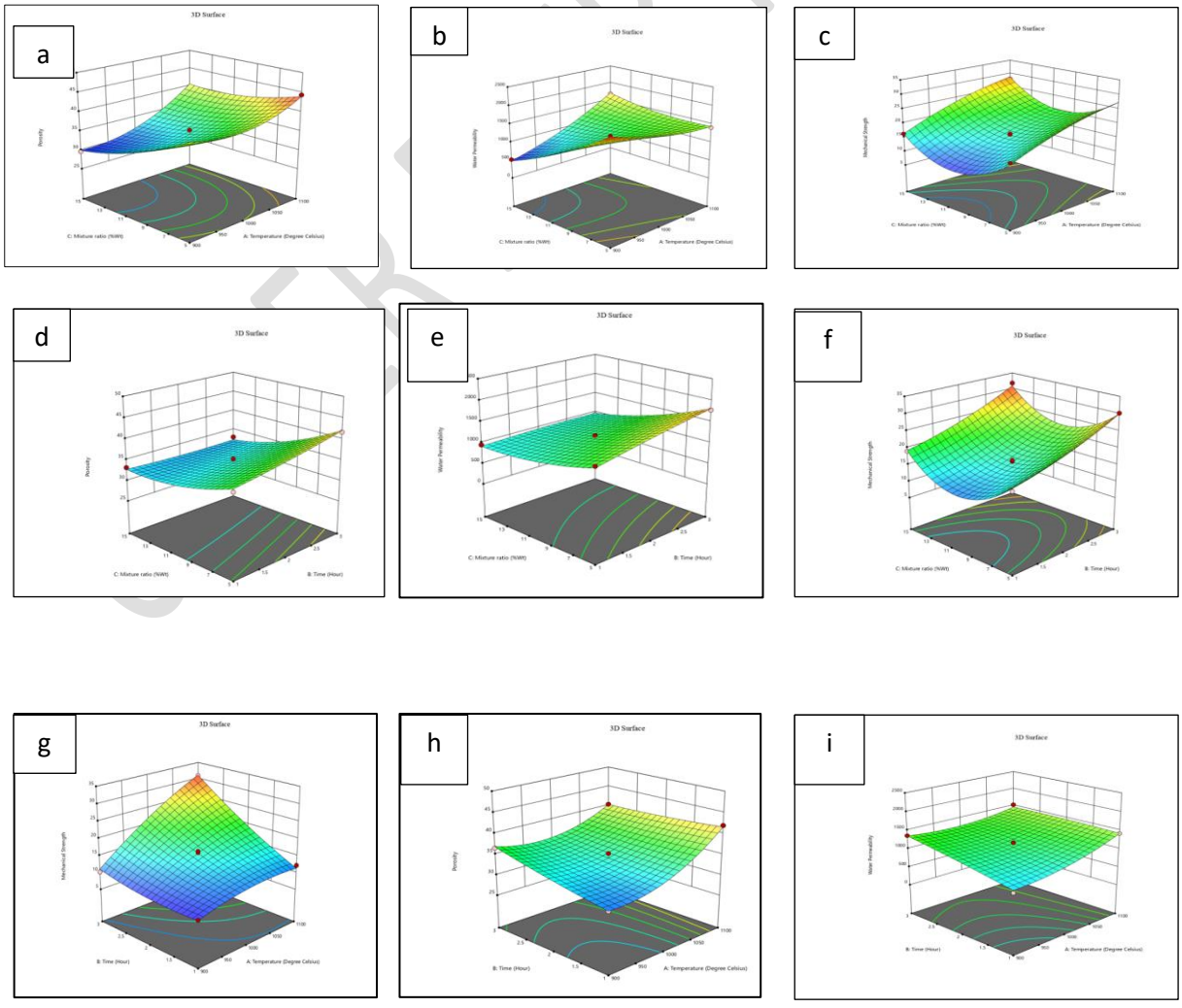

Fig. 5: 3D surface plots for porosity, water permeability and perfunctory strength of membranes

3.7 Optimization.

Variations in some interacting terms may have a positive effect on one response while having a negative effect on another. This suggests that different regions have different optimal conditions for various responses. As a result, the visual method of the 3D surface plot is no longer appropriate for locating optimal conditions. Therefore the desirability function is applied to identify the optimal conditions. Table 12 represent the boundaries on which the input factors were limited, and table 13 represent individual desirability functions for porosity, water permeability and mechanical strength of the PCMs.

Table 12: Table of constraints for optimization

Name	Goal	Lower Limit	Upper Limit	Lower Weight	Upper Weight	Importance
Factors						
A:Temperature	is in range	900	1100	1	1	3
B:Time	is in range	1	3	1	1	3
C:Mixture ratio	is in range	5	15	1	1	3
Responses						
Porosity	maximize	29.6	44.4	1	1	3

Water Permeability	maximize	522	2000	1	1	3
Mechanical Strength	maximize	8.46	31.8	1	1	3

Table 13: Individual desirability functions for porosity, water permeability and mechanical strength

Number	Temperature	Time	Mixture ratio	Porosity	Water Permeability	Mechanical Strength	Desirability	
1	**1100.114**	**3.000**	**5.000**	**44.400**	**1566.603**	**35.973**	**0.891**	**Selected**
2	1090.844	3.000	5.000	44.439	1565.463	36.012	0.890	
3	1090.734	2.977	5.000	44.400	1563.298	35.723	0.890	
4	1090.932	2.969	5.000	44.400	1562.182	35.635	0.889	
5	1093.739	3.000	5.000	44.595	1561.074	36.163	0.889	

Completely intended responses include high porosity, water permeability and mechanical strength. The optimal conditions in coded values for the mixture ratio, sintering temperature, and sintering duration are − 1, 1 and 1 respectively. It was discovered that the desirability is equal to 0.891. The equivalent true values for the kaolinite quantity, sintering temperature, and sintering duration are 5%, 1100℃, and 3 hours, respectively. To determine the obtained optimal points, validation experiments were performed using the experimental conditions reported in Table 13. Furthermore, the predicted and experimental results were compared and the residual and percentage of error values were calculated and represented in Table 14. The

highest value of porosity, water permeability and mechanical strength was 44.4%, 1566 L h^{-1} m^{-2} $bar^{-1}$and 35.97 MPa respectively while the validation experiments gave 45.9%, 1563.7 L h^{-1} m^{-2} $bar^{-1}$and 36.5 MPa . The errors (%) between the predicted and observed response values were acceptable and were within 4%.

Table 14: Optimization results

Max. Response	Temp.	MR	Time	Pred. Response	Obs. Response	Error
Porosity	1100℃	5%	3hrs	44.4%	45.9%	1.5
Permeability	1100℃	5%	3hrs	1566$Lh^{-1}m^{-2}bar^{-1}$	1563.7$Lh^{-1}m^{-2}bar^{-1}$	2.3
Mech. Strength	1100℃	5%	3hrs	35.97MPa	36.5MPa	0.53

3.8 Characterization of the optimized membrane

Using X-ray diffraction, the phase change brought on by the rising firing temperature was investigated. The findings are displayed in Figure 6. Peaks at 36.5^{o}, and 42.4^{o} that represent the mullite phase's diffraction Mullite can form at temperatures beyond 900°C, according to earlier research [43–45], and it plays a significant role in the development of mechanical strength in ceramics [46–48].These findings provide an explanation for why ceramics' compressive strength increase at high firing temperatures such as 1100°C. FTIR spectra of the membrane show the condensation of Si-OH and the thermal breakdown of rice husk as displayed in figure 7. Following firing at 1100°C, a notable vibration at 1062.3 cm^{-1} and

2158.5 cm^{-1}, corresponding to C-H bonding and the -OH group in the membrane vanished, suggesting the burning out of rice husk. And the peak at 779 cm^{-1}, indicate the condensation of Si-OH groups [41].According to Zewedie et al [49], FTIR was employed to identify the crystal structures, functional groups existing in the membrane, it can also detect other structural anomaly that may be present in the prepared membrane.

SEM micrographs of the top view of a rice husk/kaolinite optimized membrane with 500, 1000 and 2000 magnifications are displayed in Fig. 8. SEM images made it evident that the membrane was well-sintered and has a porous structure that corresponds with the porosity result. It is evident that the particles have been well-consolidated, resulting in a surface morphology that is largely uniform. According to Zou et al [50], the development of necks between grains promotes high cohesion between them, which accounts for the good mechanical strength of the optimized membrane and capacity to withstand hydraulic pressure during micro filtration. Using ImageJ software, the pore size of the rice husk/kaolinite optimized membrane was estimated on six separate top-view SEM images [51, 52].Fig.9 displays the pore size distribution of the membrane. The membrane surface has holes that are found to be between 0.14 and 3.7 µm in diameter, this shows that fabricated membrane is well positioned in the MF range. The average pore size was found to be 0.8817 µm.

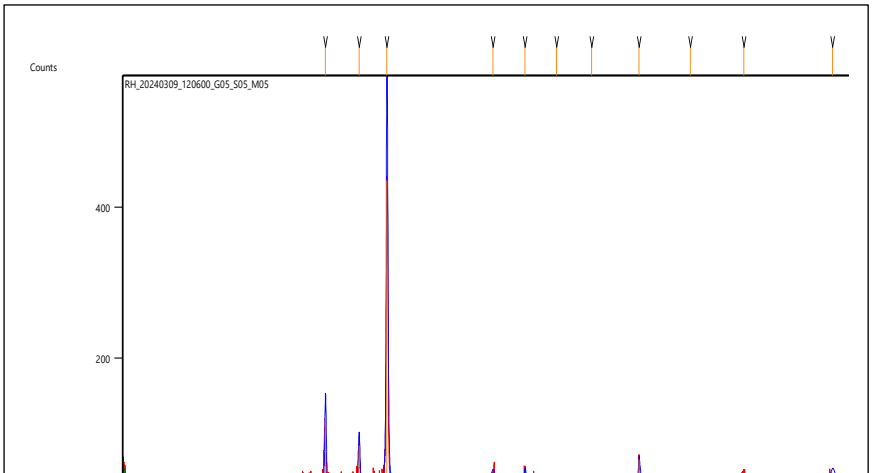

Fig. 6: XRD of Optimized Koalinite/sawdust membrane

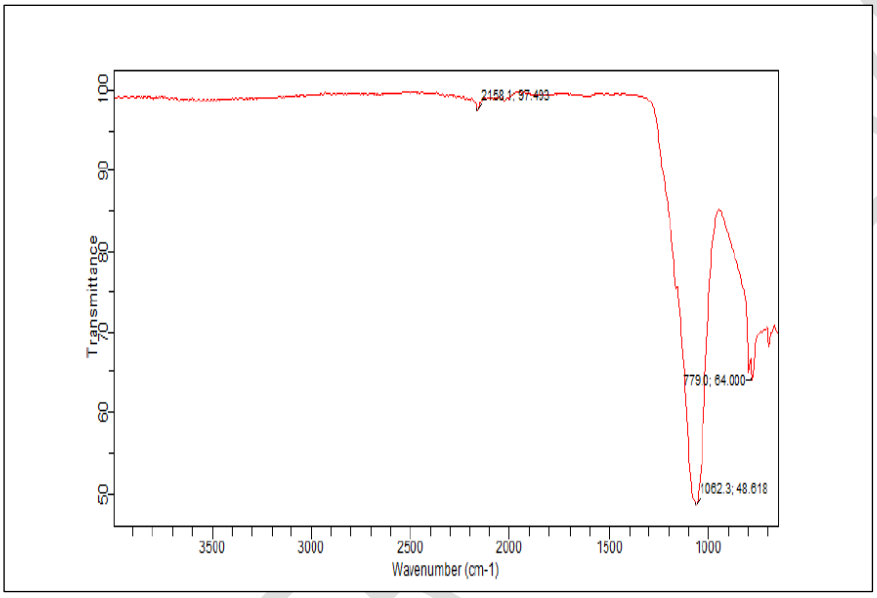

Fig. 7: FTIR representation of the optimized membrane

.

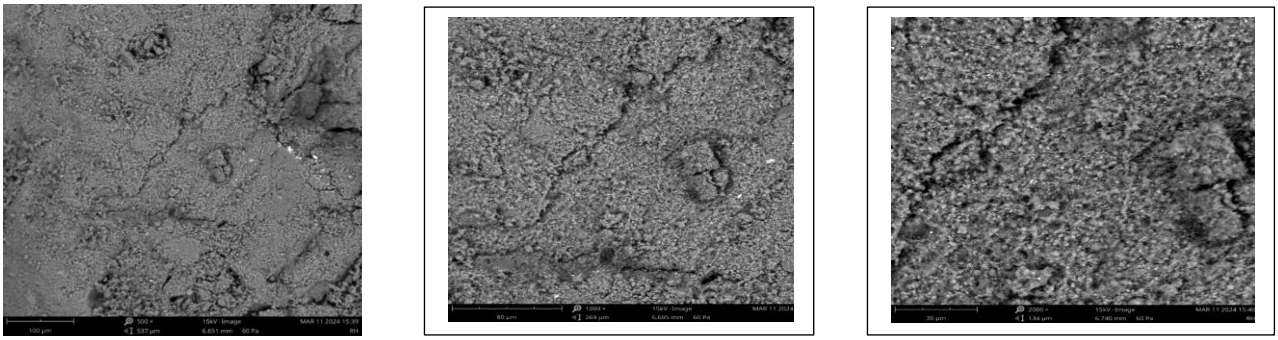

Fig. 8: SEM micrograph of Optimized membrane

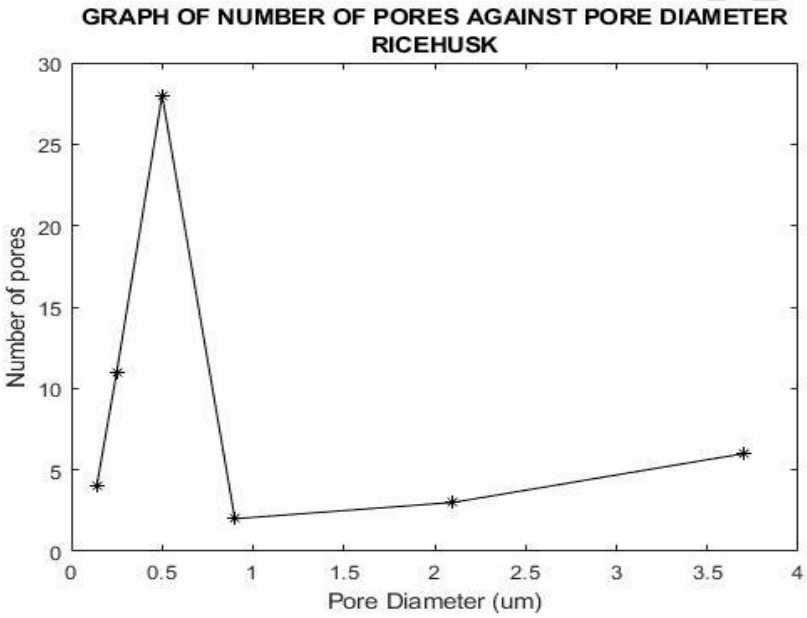

Fig. 9: Pore size distribution of the optimized membrane

3.9 Purification of Brewery water (Strike water)

Table 10 presents the physicochemical parameters of the brewery water both before and after the MF experiment. According to Eumann [8], the major properties in brewing water and their acceptable range of values are turbidity(0-0.5 NTU), dissolved solid (20-50mg/l),suspended solids (30-61mg/l), pH(5-9.5), Colour (0.00 PCU), Conductivity (25-50µS/cm), the

composition of the water used in brewing(strike water) differs depending on the type of beer being produced. In other words, the chemical properties and characteristics of are tailored to suit the specific requirements of various beer styles. However, two important elements of water will affect the taste of the beer are the pH and mineral composition. Lammers [6] also stated that any form of alkalinity in brewing water is undesirable because it interferes with the extraction process during mashing and often results in a harsher, incorrectly colored, and less enjoyable beer to drink.

Generally speaking, before mashing, the pH of brewery water should be brought to neutrality and from the results in table10, it was achieved. The flavor character of the beer is determined by the minerals in the water used for brewing. The measurement of total dissolved calcium and magnesium (TDS) is known as water hardness, and it gives beer its distinct hoppy flavor. Carbonates, sulfates, and sodium all affect how beer tastes. Throughout the brewing process, the presence (or lack) of each dissolved material will provide a distinct flavor characteristic. But, it is imperative to utilize them sparingly because an excessive quantity might result in overbearing and disagreeable flavors [6]. This water, with 28m/l is within the permissible bounds. The turbidity measures water clarity. High turbidity can lead to haze, sediment, and off-flavors in beer, as well as affect yeast performance and equipment clogging. For a good beer, turbidity is found to be below 1mg/l. In terms of TSS, Suspended particles can cause haze, sediment, and off-flavors in beer. High TSS levels can also clog brewing equipment and affect yeast performance. Conductivity measures the ability of water to conduct electricity, related to ion concentration. High conductivity can indicate high TDS levels, affecting beer flavor and quality. All these water qualities are all within the acceptable limits according to Eumann[8] who provided a standard guideline for brewery water (Strike water). On visual inspection, the water neutral color was what was needed to make a good beer, its appearance

did not necessitate further tastes. Table 10 demonstrates that 83.8%, 73%, 90.5%, and 77.7% of turbidity, TDS, TSS, and conductivity respectively can be rejected by the Nsu kaolinite/rice husk membrane.

Table 15: Physiocochemical characterization of Brewery water

Brewery water	Ph	Turbidity	Colour	TDS	TSS	Conductivity
Before	6.84	3.10	ND	104	590	160
After	6.92	0.5	ND	28	56	35.6
Rejection (%)	–	83.8	ND	73.0	90.5	77.7

Conclusion

Solid state procedure was used to create an affordable ceramic MF membrane by combining kaolinite and rice husk. RSM based on Box-Behnken design was utilized to examine the impact of experimental membrane fabrication parameters and their interactions. The optimum membrane was made with 5% kaolinite and sintered for 3 hours at 1100 ◦C. Its porosity, permeability and mechanical strength are 44.4, 1566 L h^{-1} m^{-2} $bar^{-1}$and 35.97MPa respectively. Moreover, homogenous and defect-free microstructure was shown by SEM characterization. Lastly, the filtering of borehole water into Strike water was used to evaluate the effectiveness of membrane. Its capacity to eliminate turbidity, TDS, TSS and conductivity was verified, yielding rejection rates of 83.8%, 73.00%, 90.5%, and 77.7% respectively. These results demonstrate that borehole water could be purified into brewery Strike water using the low-cost ceramic MF membrane that was synthesized.

Nomenclature

PCM	Porous ceramic membrane
RSM	Response surface methodology
MF	Microfiltration
RH	Rice husk
K	Number of factors
R_O	Number of replicates
J_w	Permeate flux($Lh^{-1}m^{-2}$)
L_p	Permeability($Lh^{-1}m^{-2}bar^{-1}$)
ΔP (bar)	Trans membrane pressure
X_f and X_p	Characterization parameters before (feed) and after (product) filtration, respectively.
TSS	Total suspended solids (mg/l)
TDS	Total dissolved solids (mg/l)

Disclaimer (Artificial intelligence)

Option 1:

Author(s) hereby declare that NO generative AI technologies such as Large Language Models (ChatGPT, COPILOT, etc.) and text-to-image generators have been used during the writing or editing of this manuscript.

Option 2:

Author(s) hereby declare that generative AI technologies such as Large Language Models, etc. have been used during the writing or editing of manuscripts. This explanation will include the name, version, model, and source of the generative AI technology and as well as all input prompts provided to the generative AI technology

Details of the AI usage are given below:

1.

2.

3.

References

1. Source FA. 2002 world beer production. BIOS International. 2003;8(2):47-50.
2. Fillaudeau L, Blanpain-Avet P, Daufin G. Water, wastewater and waste management in brewing industries. Journal of cleaner production. 2006 Jan 1;14(5):463-71.
3. H. Khaled, K. Hidouri, B. Chaouachi. Hybrid desalination combining microbial cells and reverse osmosis. JP Journal of Heat and Mass Transfer. http://dx.doi.org/10.17654/0973576322019. 26 (2022) 179-196
4. Ajari, K. Hidouri, H. Akrout, F. Khaled, B. H. Ali, B. Chaouachi, Q. Alsalhy. Improvement of a novel polymeric membrane performance by adding alumina powder for seawater desalination. Desalination and water treatment doi: 10.5004/dwt.2023.30191 (2023)
5. Bamforth C, editor. Brewing: new technologies. Woodhead Publishing; 2006 Aug 9.
6. Lammers FJ. Water Purification in the Modern Brewery and Distillery. Industrial & Engineering Chemistry. 1934 Nov 1;26 (11):1133-8.

7. Hai ZC. The impact of water quality on beer fermentation. In2011 International Conference on New Technology of Agricultural 2011 May 27 (pp. 643-645). IEEE.
8. Eumann M. Water in brewing. In Brewing 2006 Jan 1 (pp. 183-207). Woodhead Publishing.
9. Felix A, Herdegen V, Haseneder R, Härtel G, Repke JU. Investigations on the behaviour of ceramic micro-and mesoporous membranes at hydrothermal conditions. Separation and Purification Technology. 2015 Jun 25;148:85-93.
10. A. Hamzaoui, K. Hidouri, B. Chaouachi. Comparative study of the performance of a locally manufactured membrane and the commercial one in vacuum distillation (VMD) of brackish water. (2022). Desalination and water treatment doi: 10.5004/dwt.2022.28029 (2022)
11. Nandi BK, Uppaluri R, Purkait MK. Preparation and characterization of low cost ceramic membranes for micro-filtration applications. Applied Clay Science. 2008 Dec 1;42(1-2):102-10.
12. Yue X, Koh YK, Ng HY. Effects of dissolved organic matters (DOMs) on membrane fouling in anaerobic ceramic membrane bioreactors (AnCMBRs) treating domestic wastewater. Water Research. 2015 Dec 1;86:96-107.
13. Amin SK, Roushdy MH, El-Sherbiny CA. An overview of production and development of ceramic membranes.
14. Moraru C, Schrader EU. Applications of membrane separation in the brewing industry. Handbook of Membrane Separations. CRC Press, Taylor & Francis. 2009:553-79.
15. K. Hidouri, H. Togun, F. L Rashi, a. M. Abed, A.K. Hussein, B. Ali, S. Rout, M. B. B. Hamida, U. Biswal. Environmental studies for various simple and hybrid solar still

configurations : a comprehensive review. Journal of Thermal Engineering (2024) 10(6):1698-1714 DOI 10.14744/thermal.0000877.

16. H. Ajari, F. Khaled, H. Akrout, H. Khaoula, B. Chaouachi, Q. Alsalhy. Novel composite membrane based on Recycled low-density polyethylene-alumina used for vacuum membrane distillation. Bulletin of the National Research Centre (2023) indexing services including PubMed Central and Web of Science (Clarivate Analytics) ISSN: 2522-8307.
17. Farrow C, McBean E, Huang G, Yang A, Wu Y, Liu Z, Dai Z, Fu HY, Cawte T, Li YP. Ceramic water filters: A point-of-use water treatment technology to remove bacteria from drinking water in Longhai City, Fujian Province. Journal of Environmental Informatics. 2018 Dec 1;32(2):63-8.
18. Bielefeldt AR, Kowalski K, Summers RS. Bacterial treatment effectiveness of point-of-use ceramic water filters. Water research. 2009 Aug 1;43(14):3559-65.
19. Clasen TF, Brown J, Collin S, Suntura O, Cairncross S. Reducing diarrhea through the use of household-based ceramic water filters: a randomized, controlled trial in rural Bolivia. The American journal of tropical medicine and hygiene. 2004;70(6):651-7.
20. Rayner J, Skinner B, Lantagne D. Current practices in manufacturing locally-made ceramic pot filters for water treatment in developing countries. Journal of Water, Sanitation and Hygiene for Development. 2013 Jun 1;3(2):252-61.
21. Sakkas VA, Islam MA, Stalikas C, Albanis TA. Photocatalytic degradation using design of experiments: a review and example of the Congo red degradation. Journal of hazardous materials. 2010 Mar 15;175(1-3):33-44.

22. Singh RK. Methylcellulose synthesis from corn cobs: Study of the effect of solvent conditions on product properties by thermal analysis. Journal of thermal analysis and calorimetry. 2013 Nov;114:809-19.
23. Segal D. Chemical synthesis of ceramic materials. Journal of Materials Chemistry. 1997;7(8):1297-305.
24. Moore EA, Smart LE. Synthesis of Solids. InSolid State Chemistry 2020 Aug 3 (pp. 131-158). CRC Press.
25. Van Halem D. Ceramic silver impregnated pot filters for household drinking water treatment in developing countries. Delft University of Technology. 2006 Nov;1.
26. Belgada A, Charik FZ, Achiou B, Kambuyi TN, Younssi SA, Beniazza R, Dani A, Benhida R, Ouammou M. Optimization of phosphate/kaolinite microfiltration membrane using Box–Behnken design for treatment of industrial wastewater. Journal of Environmental Chemical Engineering. 2021 Feb 1;9(1):104972.
27. Mohammadi T, Pak A. Effect of calcination temperature of kaolin as a support for zeolite membranes. Separation and Purification Technology. 2003 Mar 1;30(3):241-9.
28. Hubadillah SK, Othman MH, Matsuura T, Ismail AF, Rahman MA, Harun Z, Jaafar J, Nomura M. Fabrications and applications of low cost ceramic membrane from kaolin: A comprehensive review. Ceramics International. 2018 Apr 1;44(5):4538-60.
29. Aragaw TA, Angerasa FT. Synthesis and characterization of Ethiopian kaolin for the removal of basic yellow (BY 28) dye from aqueous solution as a potential adsorbent. Heliyon. 2020 Sep 1;6(9).
30. Senoussi H, Osmani H, Courtois C, el HadiBourahli M. Mineralogical and chemical characterization of DD3 kaolin from the east of Algeria. boletín de la sociedadespañola de cerámica y vidrio. 2016 May 1;55(3):121-6.

31. Douiri H, Louati S, Baklouti S, Arous M, Fakhfakh Z. Structural and dielectric comparative studies of geopolymers prepared with metakaolin and Tunisian natural clay. Applied Clay Science. 2017 Apr 1;139:40-4.
32. Behnamfard A, Chegni K, Alaei R, Veglio F. The effect of thermal and acid treatment of kaolin on its ability for cyanide removal from aqueous solutions. Environmental earth sciences. 2019 Jul;78:1-2.
33. Garcia-Valles M, Alfonso P, Martínez S, Roca N. Mineralogical and thermal characterization of kaolinitic clays from Terra Alta (Catalonia, Spain). Minerals. 2020 Feb 7;10(2):142.
34. Tabata S, Iida H, Horie T, Yamada S. Hierarchical porous carbon from cell assemblies of rice husk for in vivo applications. MedChemComm. 2010 Aug 4;1(2):136-8.
35. Madaeni SS, Arast N, Rahimpour F, Arast Y. Fabrication optimization of acrylonitrile butadiene styrene (ABS)/polyvinylpyrrolidone (PVP) nanofiltration membrane using response surface methodology. Desalination. 2011 Oct 3;280(1-3):305-12.
36. Asfaram A, Ghaedi M, Azqhandi MA, Goudarzi A, Dastkhoon MJ. Statistical experimental design, least squares-support vector machine (LS-SVM) and artificial neural network (ANN) methods for modeling the facilitated adsorption of methylene blue dye. RSC advances. 2016;6(46):40502-16.
37. Adinarayana K, Ellaiah P. Response surface optimization of the critical medium components for the production of alkaline protease by a newly isolated Bacillus sp. J Pharm Pharm Sci. 2002 Sep 1;5(3):272-8.
38. Yetilmezsoy K, Saral A. Stochastic modeling approaches based on neural network and linear–nonlinear regression techniques for the determination of single droplet

collection efficiency of countercurrent spray towers. Environmental Modeling & Assessment. 2007 Feb;12:13-26.

39. Samhari O, Younssi SA, Rabiller-Baudry M, Loulergue P, Bouhria M, Achiou B, Ouammou M. Fabrication of flat ceramic microfiltration membrane from natural kaolinite for seawater pretreatment for desalination and wastewater clarification. Desalin. Water Treat. 2020 Aug 1;194:59-68.
40. Beqqour D, Achiou B, Bouazizi A, Ouaddari H, Elomari H, Ouammou M, Bennazha J, Younssi SA. Enhancement of microfiltration performances of pozzolan membrane by incorporation of micronized phosphate and its application for industrial wastewater treatment. Journal of Environmental Chemical Engineering. 2019 Apr 1;7(2):102981.
41. Dung TT, Nam VN, Nhan TT, Hoang BN, Hung DL, Quang DV. Utilization of Rice Husk, an Abundant and Inexpensive Biomass in Porous Ceramic Membrane Preparation: A Crucial Role of Firing Temperature. Journal of Nanomaterials. 2021 Aug 4;2021:1-7.
42. Mohamed Bazin M, Ahmad N, Nakamura Y. Preparation of porous ceramic membranes from Sayong ball clay. Journal of Asian Ceramic Societies. 2019 Oct 2;7(4):417-25.
43. Chen YF, Wang MC, Hon MH. Transformation kinetics for mullite in kaolin–Al2O3 ceramics. Journal of materials research. 2003 Jun;18(6):1355-62.
44. Li DX, Thomson WJ. Kinetic mechanisms for mullite formation from sol-gel precursors. Journal of Materials Research. 1990 Sep;5(9):1963-9.
45. Okada K. Activation energy of mullitization from various starting materials. Journal of the European Ceramic Society. 2008 Jan 1;28(2):377-82.

46. Lee WE, Souza GP, McConville CJ, Tarvornpanich T, Iqbal Y. Mullite formation in clays and clay-derived vitreous ceramics. Journal of the European Ceramic Society. 2008 Jan 1;28(2):465-71.
47. Olanrewaju A, Oluseyi AK, Das SK. The effect of MgO and Cr2O3 on mullite formation from Nigeria sourced kaolin-calcined alumina sintered compacts. InIOP Conference Series: Materials Science and Engineering 2019 Apr 1 (Vol. 509, No. 1, p. 012007). IOP Publishing.
48. Heraiz M, Sahnoune F, Hrairi M, Saheb N, Ouali A. Kinetics of mullite formation from kaolinite and boehmite. Molecular Crystals and Liquid Crystals. 2016 Mar 23;628(1):55-64.
49. Zewdie TM, Prihatiningtyas I, Dutta A, Habtu NG, Van der Bruggen B. Characterization and beneficiation of Ethiopian kaolin for use in fabrication of ceramic membrane. Materials Research Express. 2021 Nov 2;8(11):115201.
50. Zou D, Qiu M, Chen X, Drioli E, Fan Y. One step co-sintering process for low-cost fly ash based ceramic microfiltration membrane in oil-in-water emulsion treatment. Separation and Purification Technology. 2019 Feb 8;210:511-20.
51. Ouaddari H, Karim A, Achiou B, Saja S, Aaddane A, Bennazha J, El Hassani IE, Ouammou M, Albizane A. New low-cost ultrafiltration membrane made from purified natural clays for direct Red 80 dye removal. Journal of Environmental Chemical Engineering. 2019 Aug 1;7(4):103268.
52. He X, Xu W, Ding F, Xu C, Li Y, Chen H, Shen J. Reaction-based ratiometric and colorimetric chemosensor for bioimaging of biosulfite in live cells, zebrafish, and food samples. Journal of Agricultural and Food Chemistry. 2020 Sep 4;68(42):11774-81.